Quantification of the dry history of the Martian soil inferred from in situ microscopy

W. T. Pike,[1] U. Staufer,[2,3] M. H. Hecht,[4] W. Goetz,[5] D. Parrat,[2,4] H. Sykulska-Lawrence,[1] S. Vijendran,[1] and M. B. Madsen[6]

Received 4 October 2011; revised 6 November 2011; accepted 8 November 2011; published 21 December 2011.

[1] The particle size distribution (PSD) of a Martian soil sample, a useful indicator of the underlying soil formation processes, has been determined using optical and atomic-force microscopy data acquired by the Phoenix Mars lander. In particular, the presence and fraction of clay-sized particles in the PSD reflects the extent of aqueous interaction with the soil. Two size populations have been identified for the Martian sample: Larger, mostly rounded grains; and small reddish fines, notably with a very low mass proportion in the clay-size range below 2 μm. These fines reflect the smallest-scale formation processes, and indicate a single method of production for the particles up to 11 μm, a much larger value than that expected for the aqueous interaction of clay formation; this suggests the fines are predominantly the product of global aeolian weathering under very dry conditions. The proportion of clay-sized soils can be used to estimate that there has been much less than 5,000 years exposure to liquid water over the history of the soil. From the perspective of the PSD, lunar regolith, rather than terrestrial soil, is the best analog to Martian soil. A globally homogenous soil with such a PSD would be an unlikely habitat for the propagation of life on Mars. **Citation:** Pike, W. T., U. Staufer, M. H. Hecht, W. Goetz, D. Parrat, H. Sykulska-Lawrence, S. Vijendran, and M. B. Madsen (2011), Quantification of the dry history of the Martian soil inferred from in situ microscopy, *Geophys. Res. Lett.*, *38*, L24201, doi:10.1029/2011GL049896.

1. Introduction

[2] A soil's particle size distribution (PSD) can provide a history of the underlying processes in its formation, including liquid water interaction. For terrestrial soils, the finest clay-sized particles are typically formed by chemical rather than mechanical processes, and are associated with aqueous weathering accompanied by the formation of clay minerals [*Bittelli et al.*, 1999]. As the proportion of clays in a soil (both the mineral and the size fraction) depends on the conditions and length of contact with liquid water, the PSD has been used to determine the exposure of soil to liquid water: *Marchant et al.* [1996] reported that the lack of authigenic clays in the Antarctic Dry Valley ash falls points to their continuous hyperaridity since their Miocene formation, a conclusion that is consistent with other markers [*Lewis et al.*, 2008]. Clay-mineral particles are at most a few micrometers across and most commonly below a micrometer in size as their growth is restricted by the introduction of crystalline imperfections [*Meunier*, 2006]. Therefore the determination of the PSD on Earth requires sub-optical-resolution techniques such as light-scattering measurements [*Bittelli et al.*, 1999]. In this work we use a combination of optical microscopy (OM) and atomic force-microscopy (AFM) to determine the PSD of the soil at the 2008 Phoenix lander site *in situ*, including the proportion of clay-sized particles present in the soil and hence quantify the contact time of the soil, with liquid water.

[3] Phoenix landed on the northern plains of Mars within the ejecta blanket of the nearby (10 km) Heimdal crater with an estimated impact of 600 Mya [*Heet et al.*, 2009]. The albedo of $\sim$0.21 and thermal inertia of 400 $\mathrm{Jm^{-2}s^{-1/2}K^{-1}}$ at the Phoenix site are typical for the Martian surface [*Ruff and Christensen*, 2002].

[4] The microscope station of the Phoenix lander [*Hecht et al.*, 2008] was able to image the dust and soil at a much higher resolution than previous Martian missions [*Herkenhoff et al.*, 2004]. With a 4-μm pixel size for the optical microscope and better than 100 nm resolution with the AFM, the microscope station offered the highest resolution of the three Phoenix cameras [*Keller et al.*, 2008; *Smith et al.*, 2009]. The robotic-arm scoop excavated and delivered a series of soil samples from the Phoenix work area to a set of substrates for imaging by the two microscopes. Figure 1 shows the most representative OM image for each sample on a magnetic substrate [*Leer et al.*, 2008]. All the samples reveal a similar soil composition; larger grains of various colors with fines of a uniform reddish coloration [*Goetz et al.*, 2010]. The spectral properties of the reddish fines that dominate the overall spectrum are consistent with CRISM spectra of the landing region [*Bibring et al.*, 2005]. The CRISM data from across the planet indicate similar spectra at these wavelengths, consistent with a globally distributed soil of a uniform composition [*Bibring et al.*, 2005] with a visible color dominated by poorly defined nanophase ferric oxides [*Banin et al.*, 1993]. *In situ* measurements from rovers in other locations have independently established that this bright dust is part of a global soil unit [*Yen et al.*, 2005], though darkening around the Phoenix lander observed from

[1]Department of Electrical and Electronic Engineering, Imperial College London, London, UK.
[2]Institute of Microtechnology, University of Neuchâtel, Neuchâtel, Switzerland.
[3]Micro and Nano Engineering Laboratory, Delft University of Technology, Delft, Netherlands.
[4]Jet Propulsion Laboratory, California Institute of Technology, Pasadena, California, USA.
[5]Max Planck Institute for Solar System Research, Katlenburg-Lindau, Germany.
[6]Astrophysics and Planetary Science, Niels Bohr Institute, University of Copenhagen, Copenhagen, Denmark.

0094-8276/11/2011GL049896

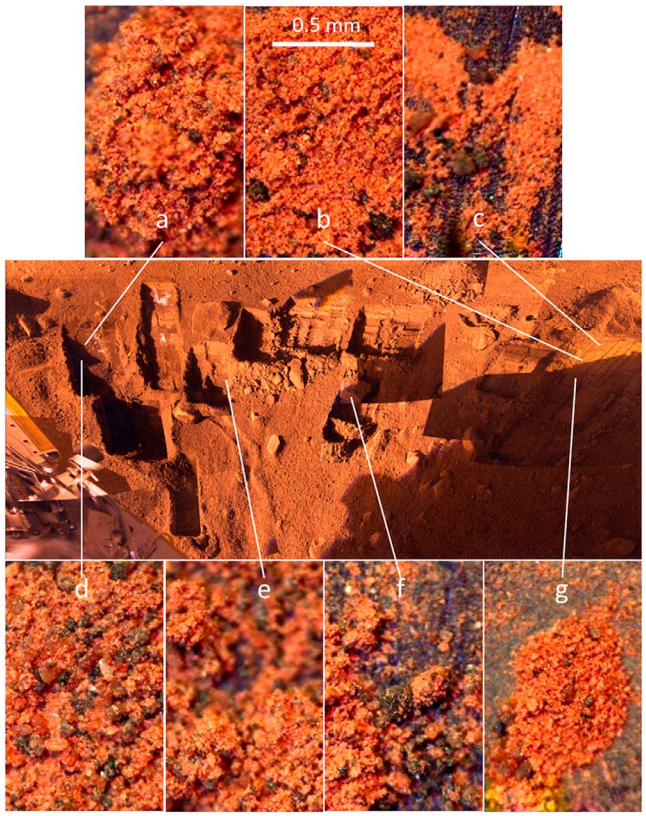

Figure 1. Micrographs of Martian soil collected from (a) Mama Bear, surface at Goldilocks trench (sol 31); (b) Rosy Red, surface near Snow White trench (sol 31); (c) Sorceress, sublimation lag from Snow White trench (sol 44); (d) Golden Key, sublimation pile from Dodo-Goldilocks trench (sol 103); (e) Golden Goose, subsurface from Stone Soup Trench (sol 112); (f) Galloping Hessian, surface sample below Headless rock near Neverland Trench (sol 132); (g) Wicked Witch, sublimation lag from Snow White trench (sol 122). Middle frame: The locations in the work area. Images of the lag deposit from the soil-rich ice in Figures 1c and 1g appear similar to the other soils, suggesting contemporaneous ice formation. Golden Key (Figure 1d) has a markedly greater proportion of large grains, indicative of entrainment of soil produced under different sorting conditions.

orbit suggests that at least some of the bright surface dust was disturbed or removed by the descent engines.

2. Approach and Results

[5] We have used OM and AFM images to determine the PSD using all the samples except Golden Key, which was not typical in appearance. In addition to images of the delivered samples, we include in our analysis images of calibration substrates that collected material inadvertently distributed within the microscope-station enclosure during the mission (a quartz calibration standard, a Macor® white calibration standard and the flat margins of micromachined silicon substrates). These images are used in combination to determine a PSD representative for the Phoenix site as a whole; the similar microscopic appearance of all the soil samples except Golden Key indicates generally uniform, well-mixed soil at this location. While the Phoenix microscope sampling mechanism rejected particles larger than 200 μm, very few particles larger than 100 μm were observed either by microscopy or from high-resolution robotic-arm-camera images at this site; the PSD of larger sand-sized particles seen in Gusev crater has been addressed by *McGlynn et al.* [2011].

[6] Particle sizes were derived from the optical images using two approaches. For the larger particle sizes, down to about 20 μm, segmentation of the individual particles was performed by hand as automated processes were unable to perform reliable thresholding on the well-populated substrates. For the smaller particles on sparsely populated substrates, automated segmentation was found to be reliable. Volumes were derived by taking the particle areas to the 3/2 power, and diameters as either the geometric mean of ellipse axes or the root of the area. We used AFM images to determine particle profiles below the OM resolution [*Hecht et al.*, 2008]. AFM images of particles on silicon and silicone substrates were individually fitted to an ellipsoid, with the highest quality AFM images selected for full analysis in three dimensions to give area and volume information. These derived volumes determined a calibration curve for all the ellipsoidally fitted particles. An example of an AFM image used for such particle size analysis is shown in Figure 2. In total 1052 particles were measured over a range of 100 nm to 200 μm in four data sets: 755 from OM by image analysis of fines on non-magnetic substrates; 186 from OM by hand, separated into two classes, grains on non-magnetic substrates and grains on magnetic substrates; and 120 from AFM images.

[7] The PSD from these measurements is derived and plotted as a relative cumulative volume against particle size rather than the more familiar histogram for both analytical and interpretative reasons; a cumulative representation of the PSD, without the binning required for a histogram, explicitly displays the contribution from every different particle size. When plotted logarithmically it also directly indicates any possible power-law relationship. Most importantly, the relative cumulative volume representation allows the different datasets to be combined under the assumption that each dataset represents a sampling from the same soil; although the proportion of the soil that provides each dataset is unknown, a combined PSD can be constructed by using the cumulative volumes of particles at the minimum and maximum size range of the dataset as two fitting parameters. These parameter pairs can be determined from the condition that both the cumulative volume and its slope should be continuous. Hence, as the AFM dataset determines the slope up to 20 μm without any initial fitting, the next overlapping dataset corresponding to the OM fines has its fitting parameters chosen to extend the PSD without discontinuity. The remaining datasets continue this process and are progressively fitted in order of increasing particle size. The final dataset, the magnetic grains that include the largest particles observed, completes the cumulative volume and thereby normalizes the volume proportion of each dataset. Undersampling of particles is evident at the lower end of the size range in the cumulative volume plots for each individual OM dataset as an unphysically steep slope. Particles in these undersampled portions of each dataset's range

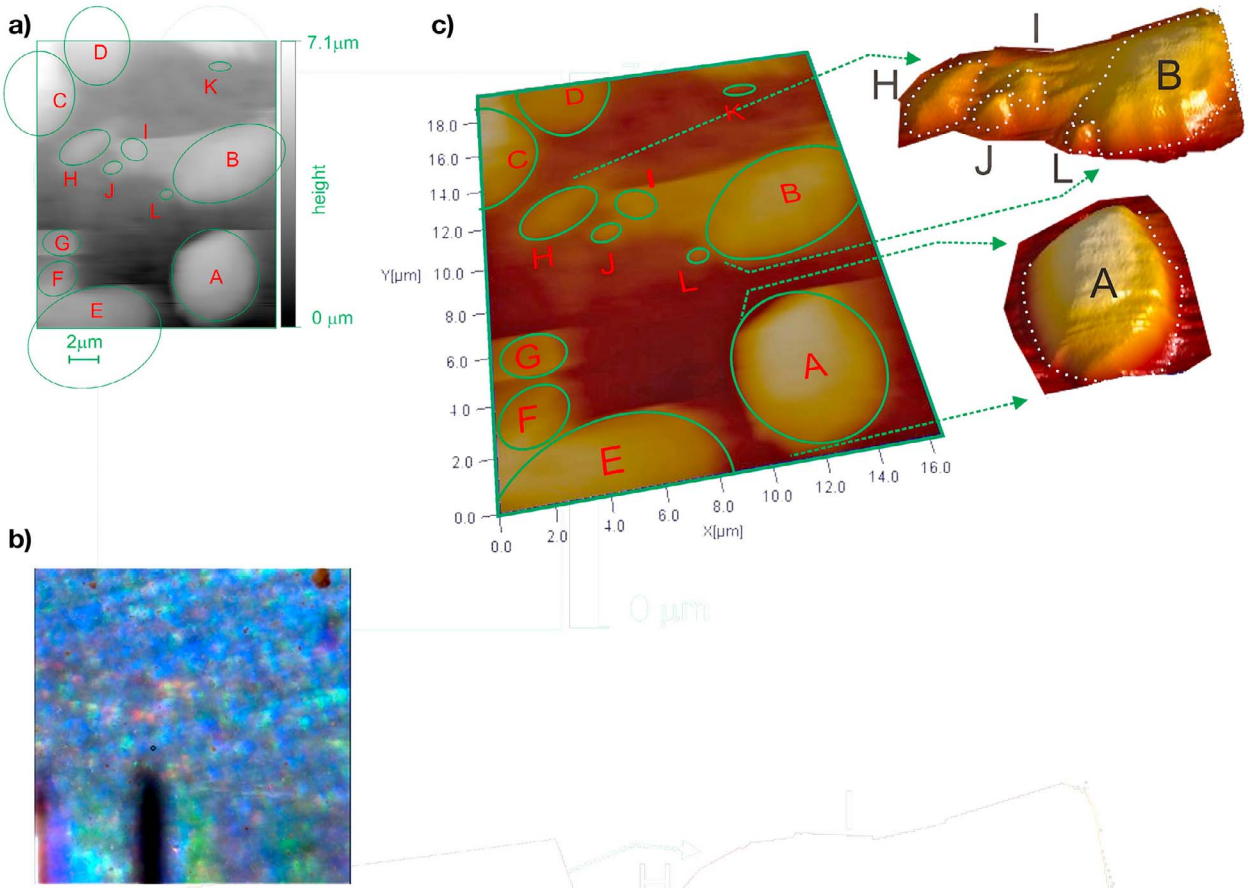

Figure 2. AFM image of particle field (a) showing top view with the ellipses fitted to each particle and (b) the same image showing the topography used to derive volumes for selected particles A and B and (c) a 1mm x 1mm OM image of the substrate with the AFM image area shown.

have been excluded from the combined OM datasets. The complete PSD of the Mars soil at the Phoenix site is shown in Figure 3.

3. Analysis

[8] The slope of cumulative volume plots can be interpreted in terms of the fractal dimension of particle fragmentation, D, inversely related to the probability of particle fracture of the soil; D can vary between the volume fractal dimension, D_V and zero, with the cumulative-volume power-law slope given by $D_v - D$ [*Turcotte*, 1986]. D_v gives the scaling law of particle volume to particle size, and as there is little evidence in OM or AFM of either fibers or plates composing much of the soil, D_v is given its usual value of 3. This analysis has been applied to terrestrial soils to separate the dominant formation processes at each length scale and provide a quantitative approach to divide the soil into sand-, silt- and clay-sized components [*Bittelli et al.*, 1999]. A fit

$$\frac{\left(\frac{x}{x_0}\right)^{3-D_0}}{1-\left(\frac{x}{x_1}\right)^{3-(D_0-D_1)}}$$

is shown for the Phoenix data with two values of the fragmentation fractal dimension, D_0 and D_1 above and below a transition size x_1. A scaling length x_0 is selected to normalize the data. D_0 has been assigned the lowest physically meaningful fragmentation fractal dimension value of zero, corresponding to "unbreakable" particles formed by the smallest-scale soil-formation process. The cumulative volume falls below this fit for the smallest particles indicating that the AFM is undersampling the particles below 1 μm. A transition at $x_1 = 11$ μm to an exponent of $D_1 = 2.25$ best fits the data. The sensitivity of the fit to x_1 is shown with two additional curves for $x_1 = 9$ and 13.5 μm.

[9] In order to verify our approach of using the Phoenix AFM images to produce the PSD plot and extract the power-law exponents, we analyzed a sample of a common Mars-soil analog, JSC Mars-1 [*Allen et al.*, 2007], in the laboratory by AFM with a functional copy of the Phoenix microscope station. For comparison purposes we also analyzed the sample with scanning electron microscopy, as has been used to determine the PSD of lunar regolith [*Park et al.*, 2008]. This end-to-end testing, which reproduced the instrumentation of Phoenix and replicated the lunar data analysis, gives good agreement between the AFM and SEM results, and in particular identifies a transition from $D_0 = 0$ to $D_1 = 1.2$ at $x_1 = 1.2 \pm 0.4$ μm (Figure 3). This corresponds to the upper

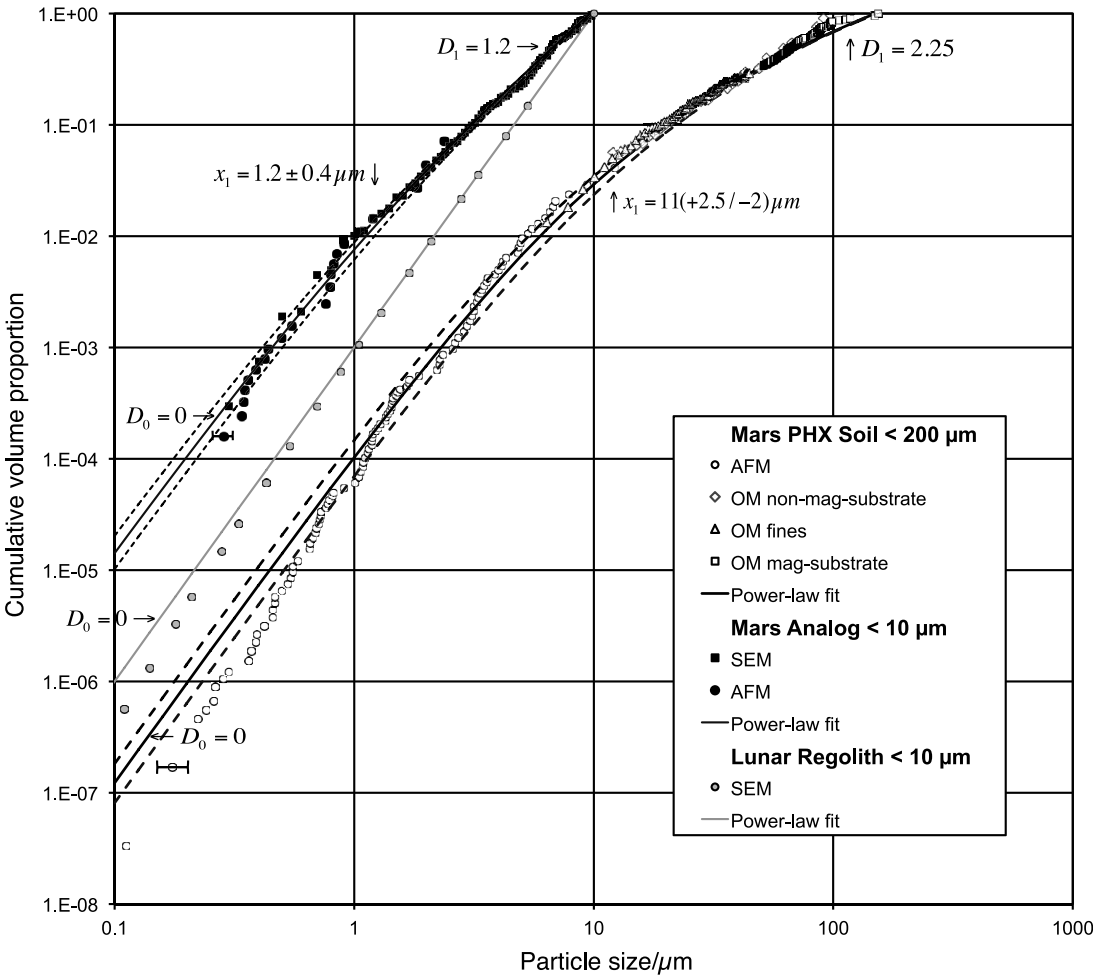

Figure 3. Particle-size distribution plotted as cumulative volume against mean particle diameter for the Mars Phoenix soil, the JSC Mars-1 analog, and lunar regolith [*Park et al.*, 2008]. Power-law relationships have been fitted to the datasets: a fragmentation fractal dimension, D_0, of for all three PSDs, with additional transitions for the Mars and analog soils at particle length scales, x_1, of 11(+2.5/−2) μm and 1.2 $\pm$ 0.4 μm to a second fractal dimension D_1 of 2.25 and 1.2 respectively.

limit of terrestrial clay formation consistent with a degree of aqueous alteration of this analog.

4. Discussion

[10] Prior studies of Martian soil properties at the particle scale have been inferential due to the lack of sufficiently high resolution imaging. Reporting on MER studies of soil at widely separated sites, Gusev crater and Meridiani planum, *Yen et al.* [2005] and *McSween et al.* [2010] found that all but the coarsest components (mm scale or larger fragments, clasts, spherules, etc.) were globally uniform – either as a result of transport or similar parent rock – and were for the most part unrelated compositionally to local outcrop rocks. Both groups reported little evidence of aqueous alteration. *Yen et al.* [2005] identified the dominant soil type as "dark," with grain sizes up to 100 μm, consistent with this work. Spectroscopically, they found the dark soil to be dominated by nanophase iron oxide (npFeOx), though they concluded that this pigment accounts for only a few percent of the total composition by mass. *McSween et al.* [2010] described the soils as a mixture of igneous and alteration phases in a ratio of ~3:1, "physical mixtures of unrelated materials" derived from rocks having different histories and ages, an olio of ancient weathering and younger comminution products with minimal if any exposure to fluids (i.e. the observed alteration *did not* occur *in situ*). *McSween et al.* [2010] further suggest that the igneous material is associated with the sand-sized component of the soil while altered materials are associated with finer dust, consistent with the present work.

[11] In our analysis, a value of D_0 indistinguishable from zero for the Martian fines up to 11 μm in size indicates that this range is the smallest-length-scale domain for formation; there can be no further break in the slope of the distribution beyond the resolution of the AFM. On Earth this domain corresponds to the aqueously produced clay-mineral fraction of the soil, with D taking a value below 1 and the upper limit of this domain generally less than one micrometer, as determined by the maximum size of clay mineral that can be formed [*Meunier*, 2006]. The mass proportion of clay minerals in terrestrial soil below this upper limit is generally above one percent due to the ubiquity of liquid water [*Bittelli et al.*, 1999]. The smallest-scale domain for the particles at the Phoenix site extends up to 11 μm, an order of magnitude larger than seen in terrestrial soils. This high value is unlikely to be an artifact of our analysis as demonstrated by the ability

to identify a much lower transition length for JSC Mars-1 with a functional copy of the flight hardware. Lunar regolith, plotted for comparison in Figure 3, has a cumulative particle mass distribution with a fractal dimension of zero for particles up to at least 10 μm in diameter [*Carpenter et al.*, 2010]: The soil at the Phoenix site is better matched in terms of PSD to lunar regolith rather than any terrestrial soil in the range up to 10 μm.

[12] The proportion of clay-sized particles can be used to provide an upper bound for the cumulative time soil has seen the liquid water necessary for their formation by assuming that all such fines are phyllosilicates. The production time for a soil with 6% phyllosilicate by volume is up to 400,000 years [*Price et al.*, 2005] based on the slowest growth rates currently observed. Hence, as less than 0.05% volume of the Martian soil is of a size consistent with phyllosilicates (less than 2 μm), this implies the soil has seen at the very most a total of 5,000 years of liquid water in its history, and probably much less. The same exposure time of 5,000 years can be calculated from Barshad's lowest value of 10^{-7} proportional phyllosilicate conversion per year observed in a wide range of soils [*Barshad*, 1957].

[13] The soil samples producing the Phoenix PSD appear to originate from a well-mixed material typical of the Martian surface. Phoenix landed in an area of Mars where neither erosion nor deposition are dominant processes, and aeolian processes are the most important transport mode. The site has an average albedo and thermal inertia. There are no signs of fractionation by depth of the soil in terms of the soil microstructure: the most notable feature of the optical microscope images taken from the Phoenix excavations is their similarity. The internal consistency of the PSD as determined by OM and AFM of different substrates further indicates that gross biasing from sample preparation is unlikely. The only biasing evident is an inability to image a representative proportion of the very finest particles as shown by the slope of the cumulative mass distribution increasing above the maximum theoretical value of three (Figure 3). Such a loss of the finest material from contributing to the PSD would produce some uncertainty in the precise fraction of the soil below a few micrometers in diameter, but would not obscure any change in the power law due to an additional soil formation process, as demonstrated by the terrestrial analysis on analog material. Hence the PSD of the fines portion of the Martian soil as determined here should be representative of the Phoenix site in particular and most likely of the Martian surface in general.

[14] There are several formation pathways that would produce the PSD we have determined without aqueous interaction. One possibility is that the smallest particle domain, below 11 μm, corresponds to many hundreds of million of years of comminution due to aeolian processes, while the particles above 11 μm, mostly grains, are the result of fracturing and melting from the Heimdal impact. The Phoenix soil therefore might have both an episodic local and continuous global origin.

[15] A water exposure time of 0–10,000 years would be consistent with observations from orbital spectroscopy that positively identified phyllosilicates in exposed Noachian formations in numerous sites across the planet, but not in the dust/soil material [e.g., *Poulet et al.*, 2005; *Mustard et al.*, 2008; *Bishop et al.*, 2008; *Murchie et al.*, 2009]. This result does not contradict mid-latitude formation of gullies through surface run-off [*Christensen*, 2003] or temporary seas [*Murray et al.*, 2005] but does suggest that the volume of soil that might have experienced such aqueous conditions over an extended period of time is a small proportion of the total soil volume of Mars, as suggested by the analysis of *Tosca et al.* [2008].

5. Conclusion

[16] If the fines component of the soil at the Phoenix site is representative of a globally distributed material, this work provides quantitative confirmation of previous chemical and mineralogical evidence from the MER locations [*Goetz et al.*, 2005] of a dry history for most of the surface material of Mars going back at least to the time of the Heimdal impact, estimated at 600 Mya. As signs of liquid-water activity are minimal as inferred here from its microstructure, the Martian soil in general would be a poor choice of sample for future investigations of past or present life.

[17] **Acknowledgments.** We dedicate this paper to the late Thomas P. Meloy, whose passion for the physics of particles defined these experiments. We thank T. Akiyama, D. Müller, S. Gautsch, H. R. Hidber, L. Howald, P. Niedermann, S. F. Hviid, J.-M. Morookian, E. Hemmig and C. Charalambos for technical assistance, and Michael Velbel and our reviewers for helpful comments on the earlier versions. Financial support from the UK Science and Technology Facilities Council, the Danish Research Agency, the Wolfermann-Nägeli Foundation, Switzerland, the Space Center at EPFL, Switzerland, the Swiss National Science Foundation, and the National Aeronautics and Space Administration is gratefully acknowledged. Part of the research reported here was carried out at the Jet Propulsion Laboratory, California Institute of Technology, under a contract with NASA.

[18] The Editor thanks Ken Herkenhoff and Peter Smith.

References

Allen, C. C., R. V. Morris, D. J. Lindstrom, M. M. Lindstrom, and J. P. Lockwood (2007), JSC MARS-1: Martian regolith simulant, *Proc. Lunar Planet. Sci. Conf., 28th*, Abstract 1797.

Banin, A., T. Ben-Shlomo, L. Margulies, D. F. Blake, R. L. Mancinelli, and A. U. Gehring (1993), The nanophase iron mineral(s) in Mars soil, *J. Geophys. Res.*, *98*, 20,831–20,853, doi:10.1029/93JE02500.

Barshad, I. (1957), Factors affecting clay formation, paper presented at 6th National Conference on Clays and Clay Minerals, Nat. Acad. of Sci., Washington, D. C.

Bibring, J.-P., Y. Langevin, A. Gendrin, B. Gondet, and F. Poulet (2005), Mars surface diversity as revealed by the OMEGA/Mars Express observations, *Science*, *307*, 1576–1581, doi:10.1126/science.1108806.

Bishop, J. L., et al. (2008), Phyllosilicate diversity and past aqueous activity revealed at Mawrth Vallis, Mars, *Science*, *321*, 830–833, doi:10.1126/science.1159699.

Bittelli, M., G. S. Campbell, and M. Flury (1999), Characterization of particle-size distribution in soils with a fragmentation model, *Soil Sci. Soc. Am. J.*, *63*, 782–788, doi:10.2136/sssaj1999.634782x.

Carpenter, J. D., O. Angerer, M. Durante, D. Linnarson, and W. T. Pike (2010), Life sciences investigations for ESA's first lunar lander, *Earth Moon Planets*, *107*, 11–23, doi:10.1007/s11038-010-9375-y.

Christensen, P. R. (2003), Formation of recent Martian gullies through melting of extensive water-rich snow deposits, *Nature*, *422*, 45–48, doi:10.1038/nature01436.

Goetz, W., et al. (2005), Indication of drier periods on Mars from the chemistry and mineralogy of atmospheric dust, *Nature*, *436*, 62–65, doi:10.1038/nature03807.

Goetz, W., et al. (2010), Microscopy analysis of soils fat the Phoenix landing site, Mars: Classification of soil particles and description of their optical and magnetic properties, *J. Geophys. Res.*, *115*, E00E22, doi:10.1029/2009JE003437.

Hecht, M. H., et al. (2008), Microscopy capabilities of the Microscopy, Electrochemistry, and Conductivity Analyzer, *J. Geophys. Res.*, *113*, E00A22, doi:10.1029/2008JE003077.

Heet, T. L., R. E. Arvidson, S. C. Cull, M. T. Mellon, and K. D. Seelos (2009), Geomorphic and geologic settings of the Phoenix lander mission landing site, *J. Geophys. Res.*, *114*, E00E04, doi:10.1029/2009JE003416.

Herkenhoff, K. E., et al. (2004), Textures of the soils and rocks at Gusev crater from Spirit's microscopic imager, *Science*, *305*, 824–826, doi:10.1126/science.3050824.

Keller, H. U., et al. (2008), Phoenix Robotic Arm Camera, *J. Geophys. Res.*, *113*, E00A17, doi:10.1029/2007JE003044.

Leer, K., et al. (2008), Magnetic properties experiments and the Surface Stereo Imager calibration target onboard the Mars Phoenix 2007 lander: Design, calibration, and science goals, *J. Geophys. Res.*, *113*, E00A16, doi:10.1029/2007JE003014.

Lewis, A. R., et al. (2008), Mid-Miocene cooling and the extinction of tundra in continental Antarctica, *Proc. Natl. Acad. Sci. U. S. A.*, *105*, 10,676–10,680, doi:10.1073/pnas.0802501105.

Marchant, D. R., G. H. Denton, C. C. Swisher III, and N. Potter Jr. (1996), Late Cenozoic Antarctic paleoclimate reconstructed from volcanic ashes in the Dry Valleys region of southern Victoria Land, *Geol. Soc. Am. Bull.*, *108*, 181–194, doi:10.1130/0016-7606(1996)108<018.

McGlynn, I. O., C. M. Fedo, and H. Y. McSween Jr. (2011), Origin of basaltic soils at Gusev crater, Mars, by aeolian modification of impact-generated sediment, *J. Geophys. Res.*, *116*, E00F22, doi:10.1029/2010JE003712.

McSween, H. Y., Jr., I. O. McGlynn, and A. D. Rogers (2010), Determining the modal mineralogy of Martian soils, *J. Geophys. Res.*, *115*, E00F12, doi:10.1029/2010JE003582.

Meunier, A. (2006), Why are clay minerals small?, *Clay Miner.*, *41*, 551–566, doi:10.1180/0009855064120205.

Murchie, S. L., et al. (2009), A synthesis of Martian aqueous mineralogy after 1 Mars year of observations from the Mars Reconnaissance Orbiter, *J. Geophys. Res.*, *114*, E00D06, doi:10.1029/2009JE003342.

Murray, J. B., et al. (2005), Evidence from the Mars Express High Resolution Stereo Camera for a frozen sea close to Mars' equator, *Nature*, *434*, 352–356, doi:10.1038/nature03379.

Mustard, J. G., et al. (2008), Hydrated silicate minerals on Mars observed by the Mars Reconnaissance Orbiter CRISM instrument, *Nature*, *454*, 305–309, doi:10.1038/nature07097.

Park, J., Y. Liu, K. D. Kihm, and L. A. Taylor (2008), Characterization of lunar dust for toxicological studies. I: Particle size distribution, *J. Aerosp. Eng.*, *21*, 266–271, doi:10.1061/(ASCE)0893-1321(2008)21:4(266).

Poulet, F., J.-P. Bibring, J. F. Mustard, A. Gendrin, N. Mangold, Y. Langevin, R. E. Arvidson, B. Gondet, and C. Gomez (2005), Phyllosilicates on Mars and implications for the early Mars history, *Nature*, *438*, 623–627, doi:10.1038/nature04274.

Price, J. R., M. A. Velbel, and L. C. Patino (2005), Rates and time scales of clay-mineral formation by weathering in saprolitic regoliths of the southern Appalachians from geochemical mass balance, *Geol. Soc. Am. Bull.*, *117*, 783–794, doi:10.1130/B25547.1.

Ruff, S. W., and P. R. Christensen (2002), Bright and dark regions on Mars: Particle size and mineralogical characteristics based on Thermal Emission Spectrometer data, *J. Geophys. Res.*, *107*(E12), 5119, doi:10.1029/2001JE001580.

Smith, P. H., et al. (2009), H_2O at the Phoenix landing site, *Science*, *325*, 58–61.

Tosca, N., A. Knoll, and S. McLennan (2008), Water activity and the challenge for life on early Mars, *Science*, *320*, 1204–1207, doi:10.1126/science.1155432.

Turcotte, D. L. (1986), Fractals and fragmentation, *J. Geophys. Res.*, *91*, 1921–1926, doi:10.1029/JB091iB02p01921

Yen, A. S., et al. (2005), An integrated view of the chemistry and mineralogy of Martian soils, *Nature*, *436*, 49–54, doi:10.1038/nature03637.

W. Goetz, Max Planck Institute for Solar System Research, D-31791 Katlenburg-Lindau, Germany.

M. H. Hecht, Jet Propulsion Laboratory, California Institute of Technology, Pasadena, CA 91109, USA. (michael.h.hecht@jpl.nasa.gov)

M. B. Madsen, Astrophysics and Planetary Science, Niels Bohr Institute, University of Copenhagen, DK-2100 Copenhagen, Denmark.

D. Parrat, Institute of Microtechnology, University of Neuchâtel, CH-2002 Neuchâtel, Switzerland.

U. Staufer, Micro and Nano Engineering Laboratory, Delft University of Technology, Delft, Netherlands.

W. T. Pike, H. Sykulska-Lawrence, and S. Vijendran, Department of Electrical and Electronic Engineering, Imperial College London, London SW7 2AZ, UK.